

## Influence of an over calcined calcium oxide-based shrinkage-compensating admixture on some properties of a self-compacting concrete

Influência de um aditivo compensador de retração à base de óxido de cálcio supercalcinado nas propriedades de um concreto autoadensável

Daiane Cassol<sup>1</sup>, Giovani Luís Rech<sup>1</sup>, Eduardo Thomazi<sup>1,2</sup> , Cláudio Antônio Perottoni<sup>1</sup>,  
Janete Eunice Zorzi<sup>1</sup> 

<sup>1</sup>Universidade de Caxias do Sul, Programa de Pós-Graduação em Engenharia e Ciência dos Materiais. Rua Francisco Getúlio Vargas, 1130, 95070-560, Caxias do Sul, RS, Brasil.

<sup>2</sup>Instituto Federal do Rio Grande do Sul, R. Avelino Antônio de Souza, 1730, 95043-700, Caxias do Sul, RS, Brasil.

e-mail: cassol.daia@gmail.com, gio.pi.rech@gmail.com, eduardo.thomazi@caxias.ifrs.edu.br, caperott@gmail.com, jezorzi@ucs.br

### ABSTRACT

The demand for self-compacting concrete grows continuously due to investments in new infrastructure, upgrades, or replacement of old infrastructure. This type of concrete can mold itself into the spaces intended for it on its own and fill them without the need for any vibration or external compaction. It must achieve three main properties: fluidity, passing ability, and resistance to segregation. Monitoring these properties, the quality, and the increase in the performance of concrete structures is essential to keep up with this growth. In this work, we explore the effect of adding a commercial over calcined calcium oxide-based compound, as a shrinkage-compensating admixture, on the properties of fresh and hardened concrete, particularly on the shrinkage and curing of self-compacting concrete specimens (SCC). Also, an experimental protocol is proposed for the electrical impedance analysis of concrete samples. Fluidity, compression, shrinkage, elastic modulus, and impedance spectroscopy tests were performed, in addition to scanning electron microscopy images. The additive slightly modifies the concrete properties in the fresh state. In hardened concrete, the compressive strength and modulus of elasticity increase, in addition to a reduction in shrinkage with 2.8% of the additive.

**Keywords:** shrinkage-compensating admixture; self-compacting concrete; mechanical properties; impedance spectroscopy.

### RESUMO

A demanda por concreto autoadensável cresce continuamente devido aos investimentos em novas infraestruturas, atualizações ou substituição de infraestruturas antigas. Esse tipo de concreto é capaz de se moldar nos espaços destinados a ele por conta própria, preenchendo estes espaços, sem a necessidade de vibração ou compactação externa. Para isso, precisa alcançar três propriedades principais: fluidez, habilidade passante e resistência à segregação. Monitorar essas propriedades, a qualidade, e aumentar o desempenho das estruturas de concreto é essencial para acompanhar esse crescimento da demanda. Neste trabalho, exploramos o efeito da adição de um composto comercial à base de óxido de cálcio supercalcinado, como aditivo compensador de retração, nas propriedades do concreto fresco e endurecido, particularmente na retração e cura de corpos de prova de concreto autoadensável (CAA). Além disso, é proposto um protocolo experimental para a análise de impedância elétrica de amostras de concreto. Foram realizados testes de fluidez, compressão, retração, módulo de elasticidade e espectroscopia de impedância, além de imagens de microscopia eletrônica de varredura. O aditivo modifica levemente as propriedades do concreto no estado fresco e, no concreto endurecido, há um aumento da resistência à compressão e do módulo de elasticidade, além da redução da retração com 2,8% do aditivo.

**Palavras-chave:** aditivo compensador de retração; concreto autoadensável; propriedades mecânicas; espectroscopia de impedância.

## 1. INTRODUCTION

Developed in Japan, self-compacting concrete (SCC) is concrete that has the ability to compact itself through its own weight with the fluidity necessary for this [1]. Therefore, the proportion between paste and aggregates must be precise to achieve the workability and mobility properties required by the SCC. Furthermore, as it has a greater volume of paste and a lower aggregate content, SCC has a very high shrinkage capacity compared to conventional concretes and, consequently, a greater tendency to crack [2, 3].

Shrinkage is the decrease in volume and is an inherent property of concrete that can occur for several reasons. Shrinkage, whether plastic, drying, or autogenous, generates cracks in concrete structures, which significantly accelerate concrete degradation and steel corrosion, compromising their useful life and design strength and increasing the interference of aggressive agents [2, 4–6]. The shrinkage in mortars and concrete can be reduced using different strategies, including modifications in the mixture proportion, reinforcement, curing, and good water/cement ratio. In addition, shrinkage compensators (SCAs) and reducing admixtures (SRAs) can reduce the harmful effects generated by shrinkage [7, 8]. While SRAs are designed to reduce the surface tension of water and thus decrease drying shrinkage, SCAs are designed to compensate for overall shrinkage through a controlled initial volume expansion. They are based on the formation of calcium hydroxide platelets ( $\text{Ca}(\text{OH})_2$ ) [9, 10].

SRAs offer an effective solution to reduce shrinkage cracks in concrete elements, particularly if the elements are cast with SCC. These additives provide lower viscosity and reduce surface tension; however, as they delay cement hydration due to their effects on pore structure, SRAs adversely affect concrete durability [2, 11].

The function of the shrinkage compensating admixture is to stimulate the appearance of compressive stresses, mitigating the tensile stresses resulting from the chemical hydration. It is known that the compensating admixture based on calcium sulfoaluminates has been applied to the Portland cement-based system to control shrinkage with significant positive effects [10–15]. Self-compacting concrete (SCC) with a compensating admixture based on calcium sulfoaluminate reduces shrinkage [16]. Until now, most of the studies described in the literature, which investigate the effects of shrinkage compensating additives in SCC, are with the sulfoaluminate-based additive [8, 9, 17]. However, the situation in an SCC system with an over-calcined calcium oxide additive may be different, so the effect and mechanism of the admixture on SCC needs to be clarified.

Shrinkage-compensating admixtures based on over calcined calcium oxide undergo an expansive reaction in converting calcium oxide to calcium ( $\text{CaO}$ ), to calcium hydroxide ( $\text{Ca}(\text{OH})_2$ ), and your volume increase by about 90% [18]. As a result of this expansive process, the concrete is subjected to compressive stresses that oppose the tensile stresses generated by the concrete shrinkage. As a result, the expansion decreases porosity and permeability, increases compressive strength, and increases adhesion between the elements [19]. The reduction of shrinkage fissures is an important factor from the point of view of concrete durability and strength. This technology was invented many years ago [20]; however, as shrinkage compensation products are not frequently used in concrete structures, little information is available about their performance and possible limitations [9, 21].

As mentioned by LI *et al.* [6], the reaction of the SCA additive based on over calcined calcium oxide is so rapid that the expansion reaches its maximum in the first hours. This means that most expansion is ineffective because it occurs during the plastic states of concrete.

It is known that the properties of concrete change significantly during the curing process. Some authors state that additives based on polycarboxylates can act by delaying cement hydration, depending on the molecular structure of the chemical compound [22–25].

Obtaining experimental results on SCC properties, produced with a commercial shrinkage-compensating admixture based on over calcined calcium oxide, both in the plastic and hardened state, contributes to the increase in knowledge about the behavior of SCC. As a result, given the wealth of information obtained by electrical impedance spectroscopy (EIS) on the temporal evolution of concrete, a sample preparation protocol for analysis by EIS was developed to monitor the concrete curing process. The fundamentals of this technique are briefly described below.

Impedance spectroscopy is a technique used to characterize the electrical behavior of materials, both in solid and liquid states. The impedance technique enables results related to dielectric properties, polarization effects, defects, microstructure, and solids' conductivity through terms involving the complex impedance as a frequency function of the applied electric field [26, 27]. In this technique, the system under study (usually between two electrodes) is subjected to a time-varying electrical potential, and the magnitude and phase of the resulting current are measured. The amplitude of the sample's impedance is obtained as the ratio voltage/current. This process is then repeated by scanning the electrical potential oscillation frequency, thus determining the phase and magnitude of the sample impedance as a function of frequency. Currently, this technique uses impedance analyzers capable of scanning frequencies in intervals spanning several orders of magnitude. Thus, both slow and fast system responses can be observed at the impedance spectrum's low and high-frequency portions,

respectively. Although impedance spectroscopy is a relatively simple and fast technique, the interpretation of results is not straightforward. The interpretation of a dielectric material impedance spectrum is based on the proposal of an equivalent circuit, where the number and nature of the elements vary according to the particular experimental conditions, composition, and microstructure of the sample [28].

In practice, with building materials, it is essential to monitor the initial strength development of concrete and mortar, both on a laboratory scale and in the field. Accurate and reliable measurements can inform the proper time for removing the formwork, loading the structural elements, and determining the quality of the batch. Therefore, electrical impedance analysis has been applied following the cure of concrete and mortar, as exemplified in what follows.

CABEZA *et al.* [29] applied differential impedance analysis to study hardened Portland cement pastes. This procedure allowed obtaining the dielectric capacitance of the cement paste, free from liquid phase contributions, allowing the electrical determination of porosity. In the paper by DÍAZ *et al.* [30], mortar samples were saturated with different solutions to quantify the microstructural changes induced by concrete weathering in nearly neutral solutions containing chlorides.

The relation between the electrical properties and the degree of saturation (DoS) of moisture in cement-based materials is related to the material's durability explored in DEY *et al.* [31]. Using simplified instrumentation, the authors take an impedance-based approach to characterize electrical properties as a DoS function. The variation of the real and imaginary parts of the impedance was investigated for saturated and partially saturated conditions at frequencies between 100–500 kHz. A circuit model was proposed to explain the behavior and calculate the conductivity and mass permittivity for various degrees of saturation.

In addition to the EIS, electrochemical impedance spectroscopy, a non-destructive detection method, has attracted attention due to many possible applications. For example, in the field of civil engineering, electrochemical impedance spectroscopy has been used mainly to evaluate the corrosion behavior of reinforcements [32, 33], concrete carburizing [34], and ion transformations in cementitious materials [35, 36]. In addition, some researchers have also used this technique to study the drying behavior of cement [37, 38].

To the best of our knowledge, there are no studies on using a shrinkage-compensating admixture based on over-calcined calcium oxide in SCC. Most studies described in the literature investigate the effects of the shrinkage compensating additive in SCC with sulfoaluminate-based admixture. Obtaining experimental results of SCC properties, produced with an over calcined calcium oxide-based shrinkage-compensating admixture, both in plastic and in the hardened state, contribute to the understanding of the properties and improvement in the performance of SCC. Therefore, in addition to the study of electrical impedance spectroscopy, this work intends to evaluate the fresh state properties of the SCC (workability and segregation), in addition to the shrinkage measures and the hard state properties (compression and elastic modulus) of samples of SCC, where one mixture was used as a reference (without additive) and in another two mixtures the percentages of compensating additive were varied. Finally, scanning electron microscopy (SEM) analysis was performed to verify the presence of cracks in the hardened state.

## 2. MATERIALS AND METHODS

### 2.1. Materials

Concrete samples were prepared using cement, coarse aggregate, fine aggregate (natural sand), and water. The coarse, medium and fine aggregates, in addition to the fine sand used in this research, were obtained from natural deposits in Rio Grande do Sul (Brazil). Natural sand was used as fine aggregate, and basaltic gravel with the commercial classification of gravel or gravel 0 (maximum dimension) was used. The characterization of aggregates is presented in Table 1, and the characterization tests were performed according to ABNT NBR NM 248, NBR NM 52, and NBR NM 53 [39–41]. High early strength cement – CPV-ARI from Itambé Cimentos – was used to prepare the samples. This choice was made because it is the type most used by precast companies [37], and for its lower content of mineral additions in its composition, made from clinker, gypsum, and carbonate material (90 to 95% clinker). The chemical properties of cement are given in Table 2.

The superplasticizer admixture was the CQ Flow 18 line – superplasticizer type SP-II, from Camargo Química. This is a third-generation superplasticizer admixture based on polycarboxylate and totally free from chlorides, with a density of 1.05 to 1.07 g/cm<sup>3</sup> and a pH ranging from 4.5 to 6.5. This admixture has several advantages, such as increasing the compressive and bending strength, decreasing the permeability, and increasing the durability of concrete. These benefits come mainly from the large reduction in mixing water needed.

The shrinkage-compensating admixture (SCA) used was from the Chimica Edile do Brasil, DRY D1 “NG” line. This product is a heat-treated, inorganic, powdered calcium oxide and is chloride-free. The firing

**Table 1:** Characterization of aggregates.

AGGREGATE	MAXIMUM DIAMETER (mm)	FINENESS MODULUS	APPARENT DENSITY (g/cm <sup>3</sup> )	UNIT MASS (g/cm <sup>3</sup> )
Fine sand	0.3	0.67	2.62	1.71
Medium sand	4.8	2.42	2.60	1.67
Gravel 0	9.5	5.86	2.54	1.62

**Table 2:** Chemical composition and some properties of CP V – ARI cement [42].

MATERIALS AND PROPERTIES		RESULTS (% wt)
Aluminum oxide	Al <sub>2</sub> O <sub>3</sub>	4.38
Silicon dioxide	SiO <sub>2</sub>	19.09
Iron oxide	Fe <sub>2</sub> O <sub>3</sub>	2.87
Calcium oxide	CaO	62.24
Magnesium oxide	MgO	3.24
Sulfuric anhydride	SO <sub>3</sub>	2.73
Loss on the ignition	LOI	3.57
Free CaO	–	1.08
Insoluble residue	–	0.77
Density (g/cm <sup>3</sup> )	–	3.09

**Table 3:** Chemical composition of the commercial shrinkage-compensating compound, normalized to 100% on a dry basis.

MATERIALS		CONTENT (% wt)
Calcium oxide	CaO	97.14
Silicon dioxide	SiO <sub>2</sub>	1.00
Magnesium oxide	MgO	1.00
Aluminum oxide	Al <sub>2</sub> O <sub>3</sub>	0.23
Iron oxide	Fe <sub>2</sub> O <sub>3</sub>	0.12
Potassium oxide	K <sub>2</sub> O	0.12
Sulfuric anhydride	SO <sub>3</sub>	0.12
Phosphorous pentoxide	P <sub>2</sub> O <sub>5</sub>	<0.12
Strontium oxide	SrO	<0.12

temperature, indicated by the company, is in a wide range between 900 °C and 1400 °C. Along with the other concrete components, the shrinkage-compensating admixture reduces the concrete porosity, increases the bonds between the aggregates and the binder, and eliminates cracking. A sample of the loose powder was characterized by X-ray fluorescence. Total semiquantitative chemical analysis was performed on an X-ray fluorescence spectrometer (Panalytical, Axios Max) at LAMIR (Laboratório de Análises de Minerais e Rochas). The results obtained are on a dry basis and are given in Table 3.

## 2.2. Methods

*Mixture proportion:* at this step, the study of the dosage of self-compacting concrete (SCC) used in the research was carried out. The dosage was based on the reference [43] method, with a pilot mixture given in Table 4. The other two mixes were prepared by varying the proportion of shrinkage compensating admixture: the first with the percentage recommended by the manufacturing company and the second increasing at 1% in relation to the first dosage, both percentages in relation to the cement mass, as given in Table 5. The mixing procedure was carried out using a concrete mixer.

As given in Table 6, a certain number of samples were molded for each test and for each dosage.

The tests of concrete in the fresh state were carried out to verify the characteristics in this state, with the addition of the SCA. The first test used the Abrams cone method to verify if the addition of SCA would change

**Table 4:** Pilot mix proportion [43].

CEMENT (kg/m <sup>3</sup> )	FINE SAND (kg/m <sup>3</sup> )	MEDIUM SAND (kg/m <sup>3</sup> )	GRAVEL 0 (kg/m <sup>3</sup> )	WATER (kg/m <sup>3</sup> )	SUPERPLASTICIZER ADDITIVE (kg/m <sup>3</sup> )
344.1	302.1	453.2	1024.3	195.4	1.70

**Table 5:** Mix proportion.

MASS PROPORTION							
NOMENCLATURE	CEMENT (kg/m <sup>3</sup> )	FINE SAND (kg/m <sup>3</sup> )	MEDIUM SAND (kg/m <sup>3</sup> )	GRAVEL 0 (kg/m <sup>3</sup> )	WATER (kg/m <sup>3</sup> )	SUPERPLASTICIZER ADDITIVE (kg/m <sup>3</sup> )	SCA (kg/m <sup>3</sup> )
Ref.	1	0.88	1.32	2.98	0.57	0.50%	–
SCA 2.8%	1	0.88	1.32	2.98	0.57	0.50%	2.80%
SCA 3.8%	1	0.88	1.32	2.98	0.57	0.50%	3.80%

**Table 6:** Number of samples for each test.

TEST	REF.	SCA 2.8%	SCA 3.8%	TESTE AGE (in days)	TYPE OF SAMPLE (mm)
	Number of samples				
Compressive strength	9	9	9	3, 7, and 28	Cylindrical – $\varnothing$ 100 × 200
Shrinkage	3	3	3	1, 2, 3, 7, 28, and 56	Prismatic – 75 × 75 × 285
Impedance spectroscopy	3	3	3	1, 2, 7, and 28	Cylindrical – $\varnothing$ 100 × 100
Elastic modulus	3	3	3	56	Prismatic – 15 × 15 × 100

the slump of the concrete and the process followed the ABNT NBR 16889:2020 standard [44]. The superplasticizer additive was added to the trace only after carrying out this test. Then, the test was carried out to determine the spreading and the flow time, which followed the ABNT NBR 15823–2:2017 [45]. Finally, the passing ability test (L-box method) was performed. The L-box method was used to determine the ability of the SCC to pass through the armor in its fresh state. The test followed the ABNT NBR 15823–4:2017 standard [46].

Tests were also carried out in the hardened state of the concrete to verify any possible alteration with the addition of the shrinkage-compensating admixture.

*Shrinkage measurement:* metal forms were used (in LMCC, laboratory at Universidade Federal de Santa Maria). In each form, 3 specimens were molded following the same order of execution of the specimen of the impedance test: 3 specimens, numbered 1 to 3 of the reference sample, in the second batch of samples, numbered 4 to 6 of the SCA 2.8% sample and for the third batch, numbered from 7 to 9 of the SCA 3.8% sample. All samples have the superplasticizer additive in their composition did not require densification, according to ABNT NBR 16834:2020 standard [47].

The specimens were kept in the LMCC laboratory at a temperature of  $23 \pm 3$  °C and relative humidity of  $55 \pm 5\%$ . The molds were wrapped in plastic film in the first 24 hours to avoid losing moisture. The shrinkage test was carried out with a digital horizontal mechanical comparator manufactured by Mitutoyo Measuring Instruments, with 0.001 mm precision. The test followed the ABNT NBR 16834:2020 standard [47]. Before molding the samples, the reading of the effective length ( $C_e$ ) between the inner ends of the mold pins was taken. The dimensional variation of each specimen was calculated as:

$$\Delta L_i = \frac{L_i - L_0}{C_e} \times 100 \quad (1)$$

where,  $\Delta L_i$  = the dimensional variation in age “ $i$ ”, expressed as a percentage (%),  $L_i$  = the reading was taken at age “ $i$ ”, expressed in millimeters (mm),  $L_0$  = the initial reading, expressed in millimeters (mm) and,  $C_e$  = the effective length, expressed in millimeters (mm).

*Compressive strength:* the samples for the compression test were molded in the LBTEC at Universidade de Caxias do Sul. The molds used were cylindrical with a diameter of 10 cm and a height of 20 cm. The compression test was carried out in a universal testing machine EMIC, model PC 200, with a nominal capacity of 2000 kN. The faces of the specimens were ground in order to smooth the surface. The test loading occurred at a constant speed of 0.50 MPa/s, according to the standard ABNT NBR 5738: 2016 and ABNT NBR 5739:2018 [48, 49]. The tests took place in three stages: 3, 7, and 28 days and on each date, nine specimens were tested, three for each dose with the determined days.

*Elastic modulus:* the dynamic elastic modulus was determined by the impulse excitation technique, according to ASTM E1876 [50], in non-destructive testing equipment (Sonelastic, Brazil) on prism-shaped samples (Table 4) vibrated in the longitudinal mode. The samples (Reference, SCA 2.8%, and SCA 3.8%) were left at room temperature until the analysis was performed, after 56 days of hydration. Three samples of each composition were tested.

The support used for the samples in the equipment is a low-density foam, on which each sample was supported (Figure 1). The CA-DP directional acoustic pickup was placed on one of the edges of the surface of the specimen (Figure 1 – extreme left). The side of the opposite surface of the sample (Figure 1 – extreme left) was hit by the impact hammer [50]. This configuration allows the characterization of the modulus of elasticity (E). Before the test, the mass (g) of each sample was measured, in addition to the dimensions of length, width, and height. Data were transferred to Sonelastic software. Three samples of each composition were tested. The test was repeated three times for each sample, and the mean and standard deviation were calculated.

*Impedance spectroscopy:* nine cylindrical samples of concrete were molded. The specimen molds were prepared in 100 mm high, 100 mm diameter PVC tubes, closed at the bottom with a standardized cap (Figure 2). The PVC tube was cut on the side to facilitate the demolding of the specimens. Two stainless steel AISI 304 plates, 12 cm (height) × 5 cm (width) × 1.5 mm (thickness), were vertically inserted into the PVC tube. A 5 mm diameter hole was drilled near the top of each steel plate to screw connecting copper wires to electrically connect the steel electrodes to the impedance analyzer (Figure 3).

The parallelism of the plates and the spacing of 5 cm between them was maintained with guide pieces fabricated with a commercial PLA (polylactic acid) filament on a 3D printer model RepRap Graber i3 (3D desktop and open-source printer), controlled by Arduino. A base piece was inserted into the bottom of the PVC tube, and two intermediate pieces were used to improve the placement of the metal plates. To ensure total parallelism of the electrode assembly, a top cover with two slits for the electrodes was added, as shown in Figures 2 and 3. The STL files used to print these 3D parts can be downloaded from [51].

The PVC tube, base, and top cover were coated with release oil. As a result, the specimen did not require vibration or blows with a rod; the concrete was immediately settled with the SCA. The samples were kept at



**Figure 1:** Sample in the elastic modulus tester.

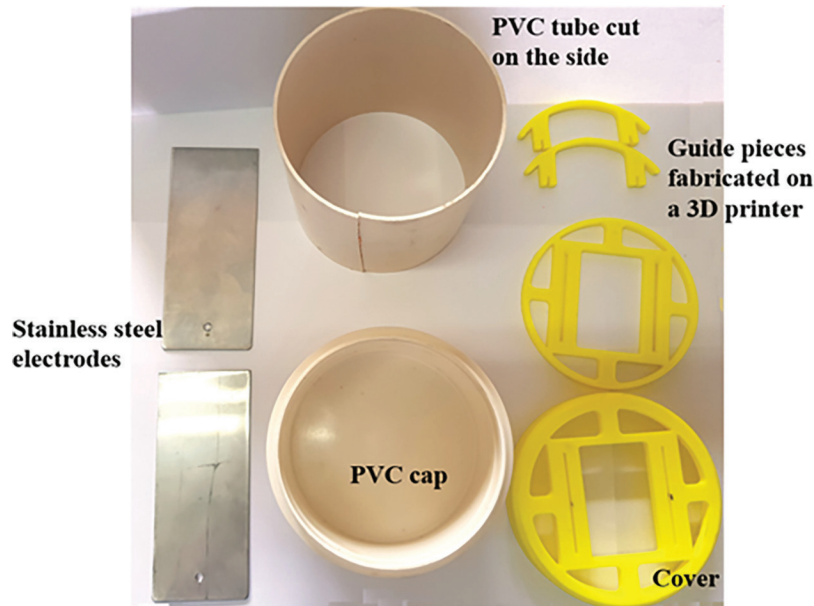


**Figure 2:** Parts used for molding the sample for EIS measurements, including stainless steel electrodes, PVC tube and cap, and 3D-printed parts (yellow).

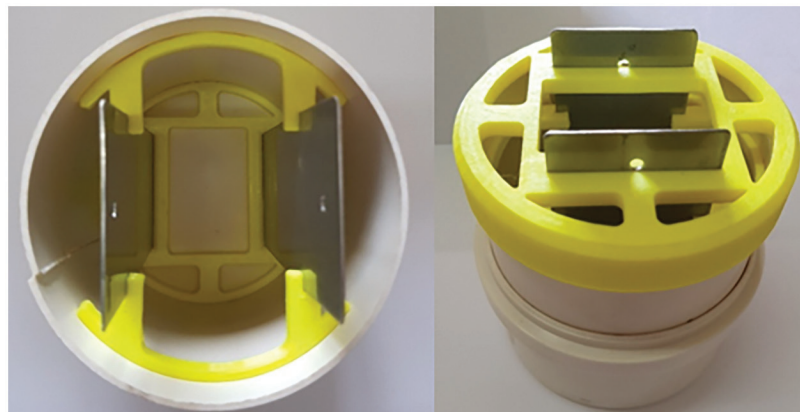


**Figure 3:** Assembly of the printed parts, in the PVC tube, with the stainless steel plates inserted in the structure.

room temperature in the laboratory for 24 hours. Then all samples were demolded, and the first round of electrical impedance measurements was performed. The samples were closed in a plastic container, with water at the bottom, to maintain the relative humidity at approximately 100%. At each measurement, the samples were removed from the container, the measurement was performed, and then the samples were returned to the box. The measurements were taken after 1, 2, 7, 33, and 56 days after the molding date.

The monitoring of the curing process was performed using electrical impedance spectroscopy (EIS), using a Precision Impedance Analyzer (Agilent, model 4294A), in the frequency range from 40 Hz to 110 MHz, with accessory 16047E. This accessory allows the connection between the impedance analyzer and the cables connected to the electrodes in the sample.

In an impedance spectroscopy experiment, a potential difference ( $V$ ), is expressed according to Equation 2.

$$V(t) = V_0 \sin(\omega t) \tag{2}$$

is applied to the electrodes inserted into the sample. In this expression,  $\omega$  is the angular frequency ( $\omega = 2\pi f$ , where  $f$  is the frequency in Hz),  $V_0$  is the signal amplitude, and  $t$  is time in s. Under the action of this potential difference, a current calculated ( $I$ ) by the Equation 3

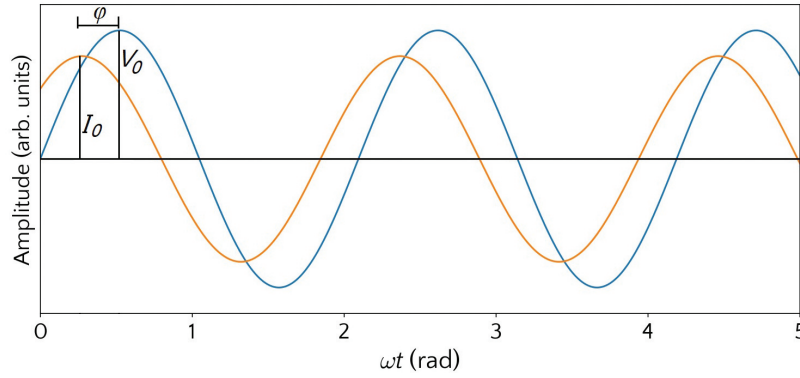


**Figure 4:** Typical time evolution of voltage (stimulus to the system) and current (measured quantity) in an EIS experiment.  $V_0$  and  $I_0$  are the applied voltage and circuit current amplitudes, respectively, and  $\varphi$  is the phase difference between voltage and current (in the sample).

$$I(t) = I_0 \sin(\omega t + \varphi) \tag{3}$$

flows through the sample, with a phase difference  $\varphi$  (between voltage and current) in relation to  $V(t)$ , as represented in Figure 4.

The complex impedance  $Z^*$  of the sample is given by

$$\begin{aligned} Z^* &= |Z| e^{-i\varphi} \\ &= |Z| \cos \varphi - i |Z| \sin \varphi \\ &= Z' - i Z'' \end{aligned} \tag{4}$$

where  $Z'$  and  $Z''$  are the complex impedance's real and imaginary part, respectively. In turn, the modulus of the sample impedance is given by

$$|Z| = \sqrt{(Z')^2 + (Z'')^2}, \tag{5}$$

and

$$\tan \varphi = \frac{Z''}{Z'}. \tag{6}$$

The results of EIS experiments are usually expressed by plotting  $-Z''(\omega)$  versus  $Z'(\omega)$ , also referred to as a Cole-Cole plot [52]. An initial measurement of a “blank sample” consisting of PVC tube plus electrodes, but without concrete/mortar (i.e., the measurement ensemble without sample), allows compensating for spurious contributions to the electrical impedance. The experimental setup for EIS analysis is represented in Figure 5.

After compensating for spurious contributions to the electrical impedance, an expression derived from an equivalent circuit model was fitted to the imaginary impedance *versus* real impedance data. The equivalent circuit, represented in Figure 6, is composed of resistors  $R_0$ ,  $R_1$ , and  $R_2$  and “constant phase elements” (CPE), with a capacitance component and an arc depression factor. This equivalent circuit for mortar/concrete samples can be interpreted in terms of an “apparent displacement resistance” ( $R_0$ ) in series with a volumetric bulk  $R_1 // CPE_1$  and an electrode network  $R_2 // CPE_2$ . The bulk resistance,  $R_b = R_0 + R_1$ , is the most reliable parameter to follow the curing reaction [52].

Assuming that the curing process is a first-order reaction [53], the reaction rate  $da/dt$  is proportional to the unreacted fraction  $(1-\alpha)$ ,

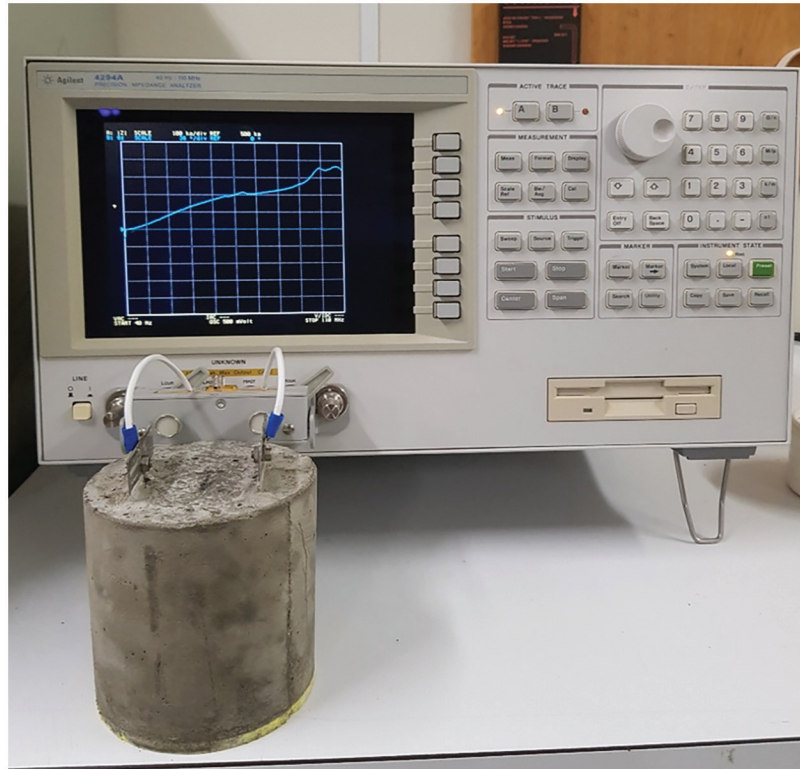


Figure 5: Experimental setup for electrical impedance measurements of concrete samples.

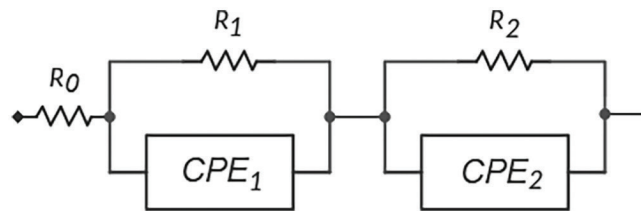


Figure 6: Electrical equivalent circuit model used to interpret results from EIS measurements on mortar and concrete [52].

$$\frac{d\alpha}{dt} = k(1 - \alpha), \tag{7}$$

where  $\alpha$  is a measure of the reaction progress ( $0 \leq \alpha \leq 1$ ), and  $k$  is the reaction constant, given by the Arrhenius equation,

$$k = A e^{\frac{-E}{RT}}, \tag{8}$$

where  $A$  is the pre-exponential factor,  $E$  is the reaction's activation energy,  $R$  is the ideal gas constant, and  $T$  is the absolute temperature.

Solving the differential equation by separation of variables we obtain,

$$\alpha(t) = 1 - e^{-kt}. \tag{9}$$

The progress of the curing reaction is obtained from the measured bulk resistance as,

$$\alpha(t) = \frac{R_b(t) - R_b(0)}{R_b(\infty) - R_b(0)}, \tag{10}$$

where  $R_b(t)$  is the sample's bulk resistance at a time  $t$  after molding, and  $R_b(0)$ ,  $R_b(\infty)$  are the corresponding values just after molding and in the limit  $t \rightarrow \infty$ , respectively. Accordingly, the variation of bulk resistance with time,  $R_b(t)$ , is given by

$$R_b(t) = R_b(0) + [R_b(\infty) - R_b(0)](1 - e^{-kt}). \tag{11}$$

Equation 11 was fitted to  $R_b(t)$  data, as obtained by impedance spectroscopy, and the progress of curing reaction was then obtained from Equation 10.

*Scanning electron microscopy:* for analysis by scanning electron microscopy, two samples of each type (Ref., SCA 2.8% and SCA 3.8%), were cut from the samples used in the elastic modulus test, coated with carbon and analyzed by backscattered electrons (BSE), with 10 keV, in a field emission gun scanning electron microscope (FEG-SEM) Mira 3 Tescan (Czech Republic).

### 3. RESULTS AND DISCUSSION

#### 3.1. Properties of fresh concrete

The slump flow test was used to verify (visually) the existence of segregation of the concrete, while the analysis of the time it took the concrete to open 50 cm (Slump Flow T50cm Test) verified whether the concrete was very or little cohesive. In addition, for each mixture, fluidity tests (spreading) were carried out for 15 minutes of mixing, verifying the loss of fluidity during this period. The results are shown in Figure 7.

Accordingly ABNT NBR 15823-1 [54], the dosages were classified as SF1 in fluidity and VS1 in viscosity, in addition to PL1 in passing ability (L box). The reference sample was classified as IEV0 (no evidence of segregation or exudation) and the samples with shrinkage compensator as IEV1 (no evidence of segregation and light exudation). The spreading diameter increased when comparing the reference sample with the two samples with the shrinkage-compensating admixture. Also, the spreading time (of 50 cm) of concrete decreases in samples with the admixture, also in an increasing way (Figure 7). Furthermore, there was no segregation regarding appearance, but exudation occurred (Figure 8). These results are in agreement with the literature [55–57].

In the work of LI *et al.* [22], immediately after mixing, the mixes with the shrinkage compensator (with a composition of 65.21% of CaO, 1.21% of MgO, and 25.32% of SO<sub>3</sub>) show a higher slump than the reference concrete. LI *et al.* [22] explain that this additive generally shows water reduction capacity due to the small air bubbles formed, which give ball-bearing effects in fresh concrete that increase the ease of movement of the aggregates at the time of mixing.

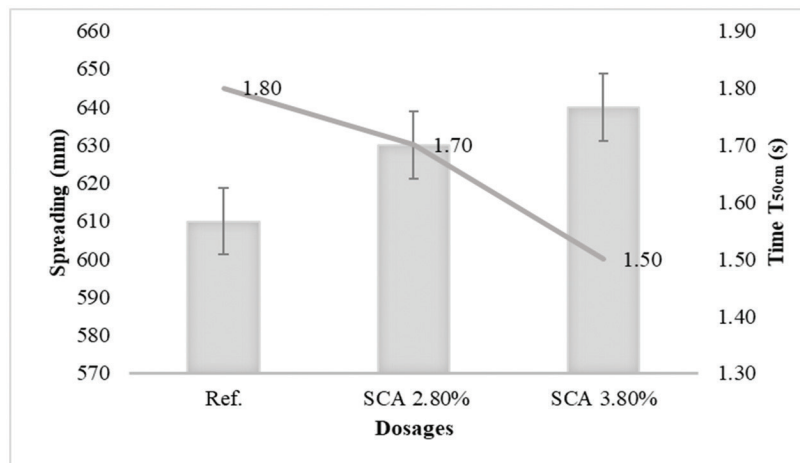


**Figure 7:** Spreading for reference sample (Ref.), SCA 2.8%, and SCA 3.8%. The continuous line refers to the time (in seconds) for the spreading to occur.

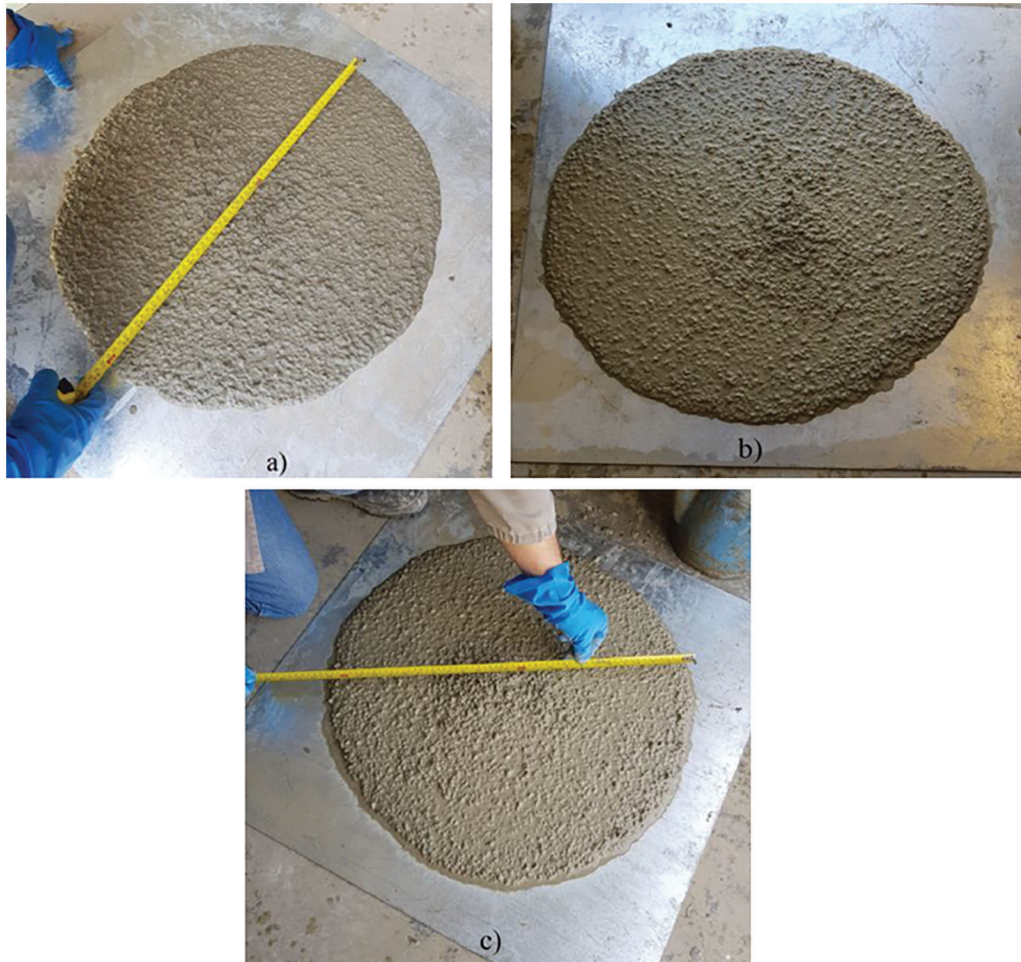


**Figure 8:** Spreading for (a) reference sample (Ref.), (b) SCA 2.8%, and (c) SCA 3.8%.

A few minutes after mixing, shrinkage compensators (with a composition of 68.5% CaO, 0.9% MgO, and 18.2% SO<sub>3</sub>) [58] showed reductions in spreading values in high-performance self-compacting concretes (HPSCCs). This phenomenon also occurs in reference [22]. Both authors cite that, possibly, this is because the compensators accelerate hydration while consuming part of the water in the mixture, followed by the formation of ettringite, which, due to its morphology, increases the resistance to flow.

### 3.2. Shrinkage measurements

The final result is presented in percentage as recommended by ABNT NBR 16834 (2020) standard [44] (Figure 9). It is noticed that the SCA 2.8% samples had a slight difference in the retraction in relation to the other samples (Ref. and SCA 3.8%), mainly in the initial ages.

According to the literature, the expansion of CaO-based additives occurs in the first 30 hours after the curing start (where, in this work, measurements were not performed) and, only after this period, the shrinkage begins. Autogenous shrinkage occurs from the initial setting while drying shrinkage starts only after 1 day when the plastic film is removed [57, 59]. Therefore, the use of CaO-based expanding agents, combined with an initial strength concrete (CP V ARI), turns out to be more advantageous for the shorter period of wet cure time (1–2 days *versus* 5–7 days) needed to develop completely the potential expansion [60].

Although the results are consistent with previous studies [10, 61–63], they differ from what is found in the studies by LI *et al.* [22] in the case of a sample with a more significant amount of SCA. In this work, the shrinkage decreases as the expander additive dosage increases.

### 3.3. Compressive strength

Compressive strength tests were performed for each sample for three specimens at 3, 7, and 28 days (Figure 10). With the SCA incorporation, the hydration acceleration period occurs after approximately 18 hours, which

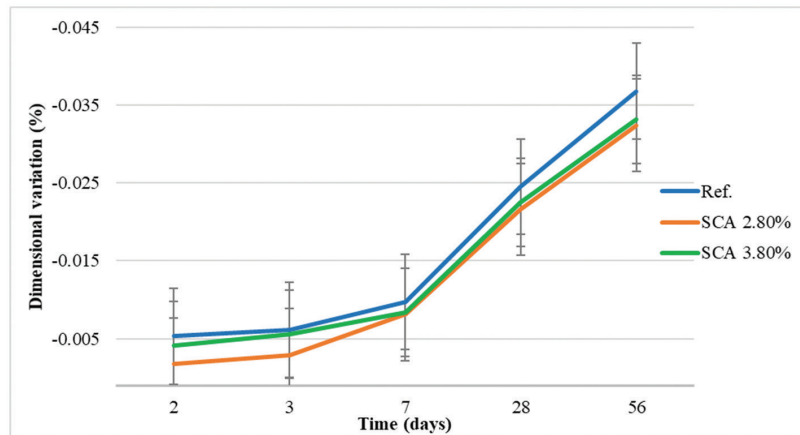


Figure 9: Shrinkage test results for Ref., SCA 2.8%, and SCA 3.8%.

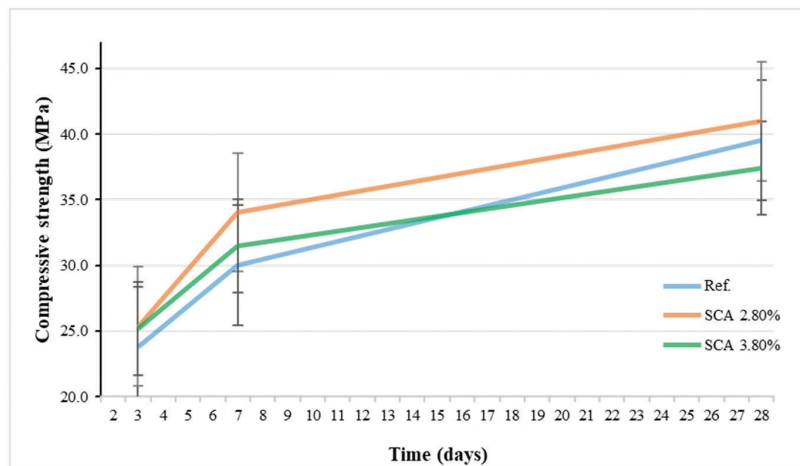


Figure 10: Compressive strength for Ref., SCA 2.8%, and SCA 3.8%.

negatively affects the mechanical strength in the first 24 hours. Since the addition of SCA delays the start of the acceleration period, the elastic modulus and compressive strength are also influenced, especially in the first 3 days of age [10, 64]. At all ages, the addition of shrinkage-compensating admixture in the percentage of 2.80% contributed to a small increase in the compressive strength of the samples. Compared with the reference sample, the incorporation of 2.80% of SCA contributed positively to the development of strength with age of cure. Samples containing 3.80% SCA had similar compressive strengths to the reference sample, but at 28 days, the addition of 3.80% had a small negative effect on strength. The results obtained agree with what was exposed by SEO *et al.* [61], where the oyster shell powder that the author used as an additive was calcined at 1000 °C. In the study by SEO *et al.* [61], the oyster shell was crushed and calcined in an electric oven at 1000 °C for 3 hours, generating material with 98% calcium oxide, a material with a composition similar to that of the SCA used in this work.

We have a contradiction in LI *et al.* [22] since the reference sample had the highest compressive strength. The author explains that this contradictory phenomenon can be attributed to the different roles of the expander additive in early and middle age. The strength in the first days is affected by the rapid formation of ettringite, which competes and inhibits the formation of C-S-H gel (the main product that contributes to the cementitious property of concrete). The inhibited formation of C-S-H causes a coarse pore structure and, consequently, a decrease in compressive strength. It should be noted that the amount of CaO in the additive used by LI *et al.* [22] and in the study carried out in this work are different.

### 3.4. Elastic modulus

When considering the same amount of mortar content in the mixture, the elastic modulus of self-compacting concretes is slightly higher than conventional concretes due to compaction and homogeneity of the mixtures

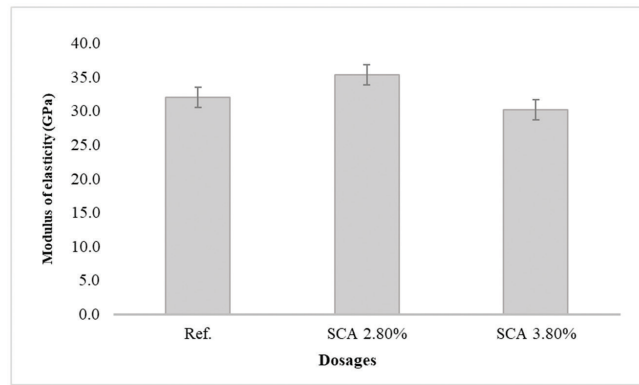


Figure 11: Elastic modulus for Ref., SCA 2.8%, and SCA 3.8%.

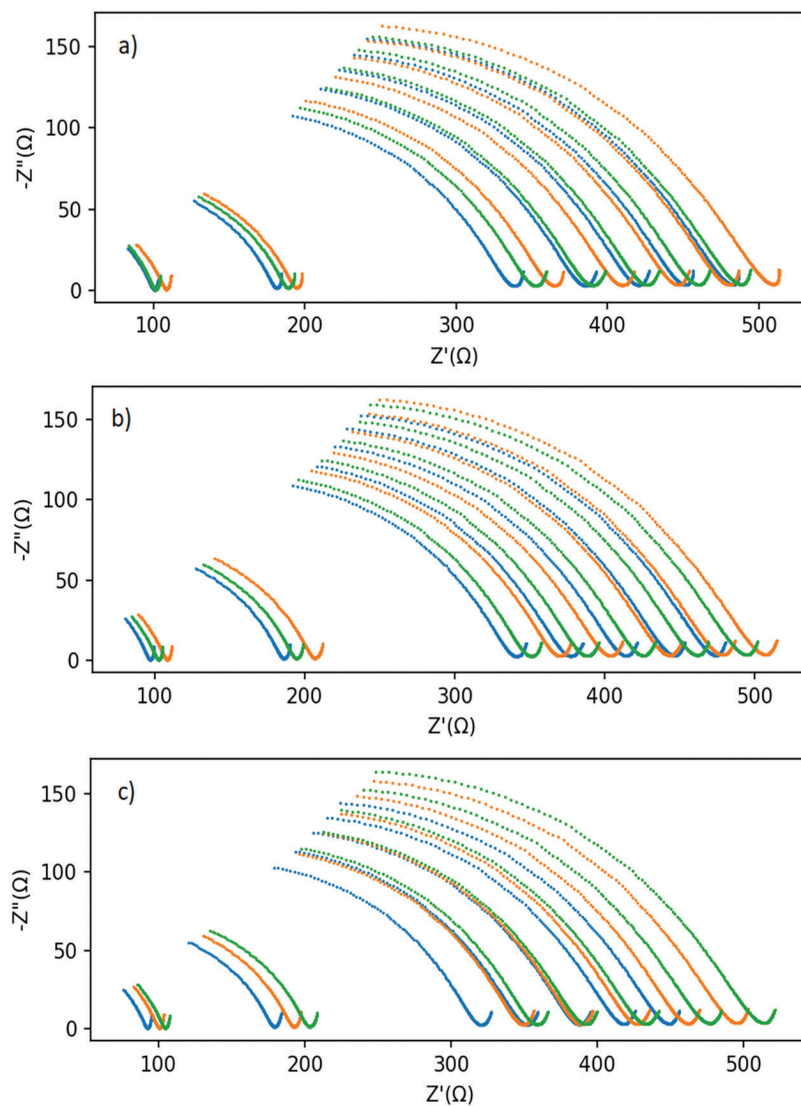
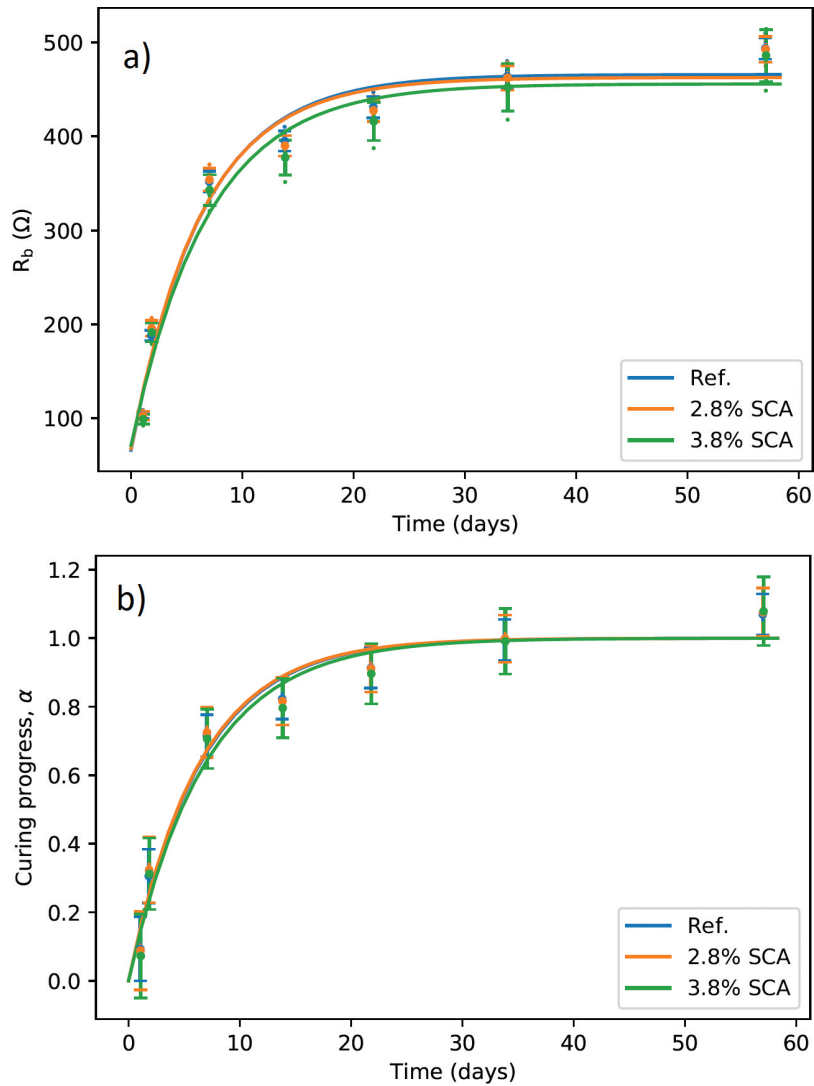


Figure 12: Cole-Cole plots show the EIS results for (a) Ref., (b) SCA 2.8%, and (c) SCA 3.8%.

[64]. Therefore, it was expected that the elastic modulus of the three dosages would be around 25–30 GPa, considering the typical values of application in the calculation of structures (Figure 11). The results obtained are similar to those found by SEO *et al.* [61]. In the research carried out by SOUZA *et al.* [10] the results obtained for compressive strength and modulus of elasticity were also similar to those of this work.



**Figure 13:** Time evolution of (a) bulk resistance,  $R_b$ , and (b) reaction progress ( $\alpha$ ) for Ref., SCA 2.8%, and SCA 3.8% samples. The solid lines represent the adjustments of (a) Equation 11, and (b) Equation 9 to the experimental data.

In work by SEO *et al.* [61] the oyster shell powder used as an additive was calcined at 1000 °C. As the firing temperature of the additive used in this work, according to the supplier, is in a wide temperature range (900 to 1400 °C), it can be considered that this temperature variation may be responsible for the results having, in general, the same behavior of the material used in SEO *et al.* [61] work. Strictly speaking, this material can only be considered over-calcined near the upper-temperature limit, i.e., 1400 °C.

### 3.5. Impedance spectroscopy

The electrical impedance after 1, 2, 7, 33, and 56 days for samples with SCA (2.8% and 3.8%) and reference are represented in Figure 12. All measurements were made in triplicate. The minimum point in these semi-arcs corresponds to the sample's bulk resistance ( $R_b$ ), which increases during the curing progress, as shown in Figure 13.

The different sets of curves for each condition (in triplicate) correspond, from left to right, to results obtained 1, 2, 7, 33, and 56 days after molding. A different color identifies each sample.

The continuous lines in Figure 12(a) represent the fitting of Equation 11 to the  $R_b$  data, from which the fit parameters  $k$ ,  $R_b(0)$ , and  $R_b(\infty)$  are obtained. The curing reaction progress  $\alpha(t)$ , was then calculated from the bulk resistance  $R_b(t)$  and the fitted parameters  $k$ ,  $R_b(0)$ , and  $R_b(\infty)$  using Equation 10 and represented in Figure 12(b). The good quality of the fitting gives support to the hypothesis that the concrete cure reaction obeys first-order kinetics. As it can be seen, the SCA does not affect the concrete's curing kinetics [65]. Moreover, python notebook used for data analysis is openly available, making it easier to replicate this work [66].

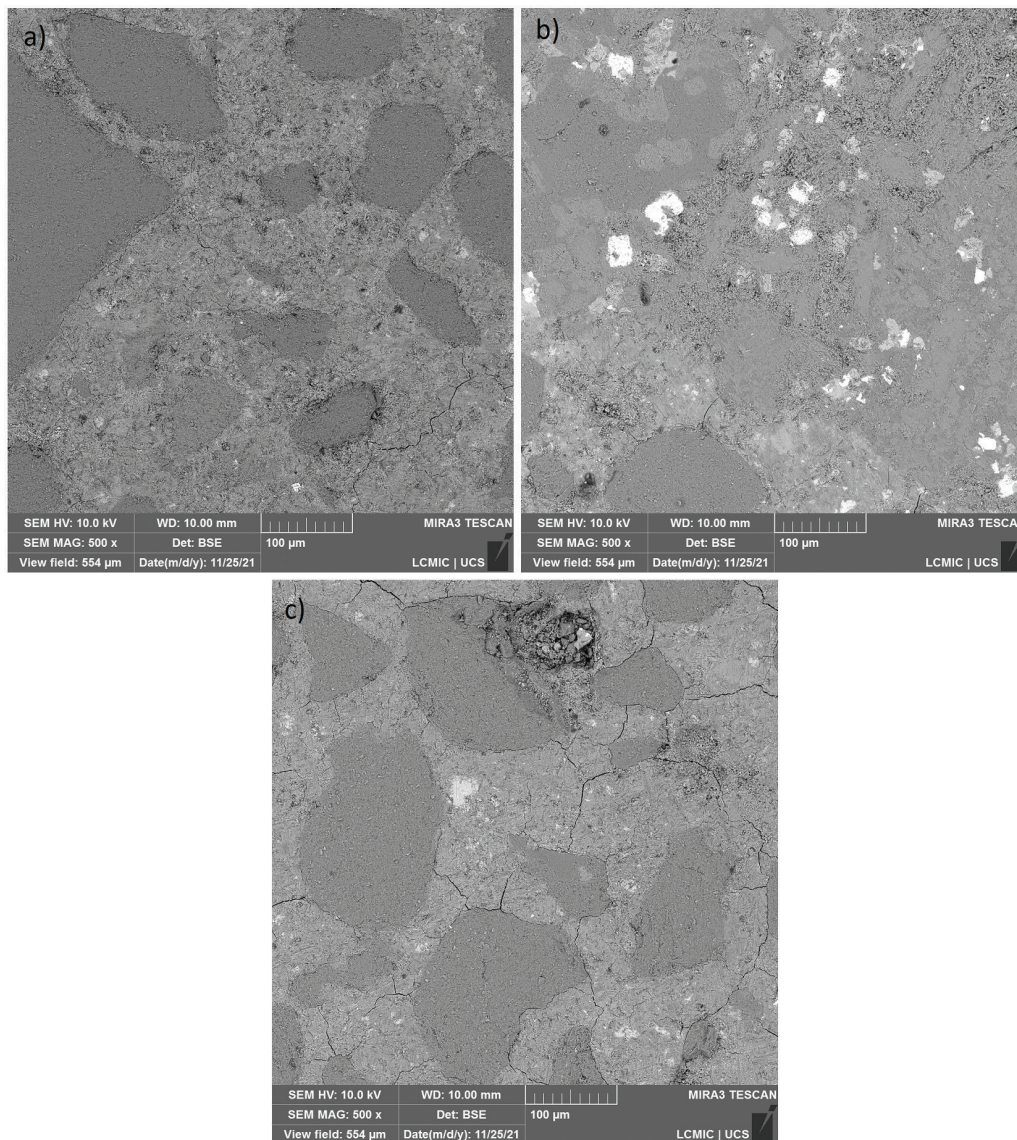


**Figure 14:** SEM images of concrete. (a) Ref., (b) SCA 2.8%, and (c) SCA 3.8%.

The Cole-Cole plots were obtained for each composition, from which we extracted the bulk resistance  $R_b$  and, from its time evolution, the curing progress. Compressive strength measurements corroborated the EIS results, with a strong correlation between bulk electrical resistance and the results of the mechanical tests. This correlation manifests itself equally for samples with and without additive.

Previous results suggest that the shrinkage-reducing admixture affects cement hydration and setting time mainly in the first 24 hours after mixing [58], in good agreement with the results represented in Figure 13(b), which show a marked progress in cure behavior during the first days after mixing.

### 3.6. Scanning electron microscopy

Figure 14 shows scanning electron microscopy (SEM) micrographs for reference (Ref.), SCA 2.8%, and SCA 3.8%, with 63 days of age. Images obtained by SEM also can provide the basis for assessing phases in concrete [67].

Fissures were observed in all samples, being slightly more significant with the increased amount of calcium oxide. According to the literature [61], in the cement hydration process, the incorporation of calcined CaO powder increased the heat of hydration in the initial stage of the reaction, forming  $\text{Ca}(\text{OH})_2$ , which may have led the sample to 3.8% to present more fissures than the others. The greater amount of fissures in the SCA 3.8% samples may be responsible because the properties, in general, are inferior to those presented by the SCA 2.8% sample.

#### 4. CONCLUSIONS

This work presents the incorporation of a commercial over-calcined CaO-based shrinkage-compensating admixture (SCA) to self-compacting concrete (SCC) and the effects this material causes on the properties of fresh and hardened concrete, in addition to its influence on the curing process. Based on the survey results, the following conclusions can be drawn:

- The fluidity, viscosity and passing ability properties fall into the SF1, VS1 and PLI classes for all grades of concrete mix. The reference sample was classified as IEV0 (no evidence of segregation or exudation), and the samples with SCA as IEV1 (no evidence of segregation and light exudation).
- As the shrinkage measurements were performed 48 h later, none of the samples presented expansion and all presented retraction.
- The sample with 2.80% of SCA had a slight reduction in shrinkage when compared to the reference sample.
- The addition of two percentages of the SCA additive to the SCC about the reference samples achieved slightly higher mechanical strength and modulus of elasticity, suggesting that the dosage is adequate.
- The incorporation of CaO as SCA did not influence the curing process of the samples.

In short, considering the incorporation of SCA into the SCC, the addition of SCA improves its workability and increases its fluidity. The mixture with the highest passing ability in the L-box test was CR 3.8%. However, there was an indication of exudation in the SCA 3.8% sample, in addition to this sample showing greater fissures, as indicated in the SEM image. Slightly better results for the shrinkage test were obtained with the 2.8% SCA samples. The same applies to the results of compressive strength and modulus of elasticity, which can be associated with the SEM image of the sample showing fewer fissures. Additional tests are needed to determine the relationship between the amount of CaO and the fissures observed. For future work, there is a need to verify the actual calcination temperature while obtaining calcium oxide.

#### 5. ACKNOWLEDGEMENTS

The support from the Brazilian Government Agencies Conselho Nacional de Desenvolvimento Científico e Tecnológico (CNPq) – grants 305528/2018-1 and 305253/2018-2. Programa de Apoio a Núcleos de Excelência (PRONEX), Fundação de Amparo à Pesquisa do Estado do Rio Grande do Sul (FAPERGS), and Universidade de Caxias do Sul (UCS) is gratefully acknowledged. This study was also financed in part by the Coordenação de Aperfeiçoamento de Pessoal de Nível Superior – Brasil (CAPES) – Finance Code 001 and Financiadora de Estudos e Projetos (FINEP). The authors would like to thank the Laboratório Central de Microscopia (LCMIC), Laboratório de Tecnologia Construtiva (LBTEC), Laboratório de Física de Materiais of the Universidade de Caxias do Sul and LMCC, laboratory at Universidade Federal de Santa Maria.

#### 6. BIBLIOGRAPHY

- [1] SANJAY, S.S., PAL, A., CHAKRABORTY, S.K., *et al.*, “Reduction of shrinkage of self-compacting concrete using polycarboxylate ether as shrinkage reducing admixture”, *Materials Today: Proceedings*, v. 60, pp. 448–451, Feb. 2022. doi: <http://dx.doi.org/10.1016/j.matpr.2022.01.316>.
- [2] SEVIM, O., KALKAN, İ., DEMIR, İ., *et al.*, “Effects of the sole or combined use of chemical admixtures on properties of self-compacting concrete”, *Archives of Civil and Mechanical Engineering*, v. 21, n. 4, pp. 1–14, Sep. 2021. doi: <http://dx.doi.org/10.1007/s43452-021-00302-7>.
- [3] LIU, K., SHUI, Z., SUN, T., *et al.*, “Effects of combined expansive agents and supplementary cementitious materials on the mechanical properties, shrinkage and chloride penetration of self-compacting concrete”, *Construction & Building Materials*, v. 211, pp. 120–129, Mar. 2019. doi: <http://dx.doi.org/10.1016/j.conbuildmat.2019.03.143>.
- [4] GIROTTO, L.S., BARBOSA, M.P., MACIEL, G.F., “Avaliação do comportamento reológico na retração plástica e na fissuração de argamassas de concreto auto-adensável”, *Revista IBRACON de Estruturas e Materiais*, v. 7, n. 1, pp. 24–52, Feb. 2014. doi: <http://dx.doi.org/10.1590/S1983-41952014000100003>.
- [5] CARBALLOSA, P., CALVO, J.G., REVUELTA, D., “Influence of expansive calcium sulfoaluminate agent dosage on properties and microstructure of expansive self-compacting concretes”, *Cement and Concrete Composites*, v. 107, pp. 103464, Mar. 2020. doi: <http://dx.doi.org/10.1016/j.cemconcomp.2019.103464>.

- [6] LI, J., ZHUANG, L., LIU, Z., *et al.*, “Evaluation of cracking in the shrinkage-compensating concrete with freeze–thaw resistance: from materials to structures”, *Materials and Structures*, v. 55, n. 5, pp. 141, May. 2022. doi: <http://dx.doi.org/10.1617/s11527-022-01982-0>.
- [7] MELO, A.A.N., CINCOTTO, M.A., REPETTE, W.L., “Efeito do aditivo compensador de retração (SCA) no cimento Portland de alta resistência inicial”, In: *Anais do 49º Congresso Brasileiro do Concreto (IBRACON)*, Bento Gonçalves, Set. 2007.
- [8] GUO, J., ZHANG, S., QI, C., *et al.*, “Effect of calcium sulfoaluminate and MgO expansive agent on the mechanical strength and crack resistance of concrete”, *Construction & Building Materials*, v. 299, pp. 123833, Sep. 2021. doi: <http://dx.doi.org/10.1016/j.conbuildmat.2021.123833>.
- [9] COLLEPARDI, M., BORSOI, A., COLLEPARDI, S., *et al.*, “Effects of shrinkage reducing admixture in shrinkage compensating concrete under non-wet curing conditions”, *Cement and Concrete Composites*, v. 27, n. 6, pp. 704–708, Jul. 2005. doi: <http://dx.doi.org/10.1016/j.cemconcomp.2004.09.020>.
- [10] SOUZA, M.T., ONGHERO, L., CORREA, B.N., *et al.*, “Novel low-cost shrinkage-compensating admixture for ordinary Portland cement”, *Construction & Building Materials*, v. 230, pp. 117024, Jan. 2020. doi: <http://dx.doi.org/10.1016/j.conbuildmat.2019.117024>.
- [11] DEMIR, İ., SEVİM, Ö., TEKİN, E., “The effects of shrinkage-reducing admixtures used in self-compacting concrete on its strength and durability”, *Construction & Building Materials*, v. 172, pp. 153–165, May. 2018. doi: <http://dx.doi.org/10.1016/j.conbuildmat.2018.03.250>.
- [12] CHAUNALI, P., MONDAL, P., “Physico-chemical interaction between mineral admixtures and OPC–calcium sulfoaluminate (CSA) cements and its influence on early-age expansion”, *Cement and Concrete Research*, v. 80, pp. 10–20, Feb. 2016. doi: <http://dx.doi.org/10.1016/j.cemconres.2015.11.003>.
- [13] JIA, Z., YANG, Y., YANG, L., *et al.*, “Hydration products, internal relative humidity and drying shrinkage of alkali activated slag mortar with expansion agents”, *Construction & Building Materials*, v. 158, pp. 198–207, Jan. 2018. doi: <http://dx.doi.org/10.1016/j.conbuildmat.2017.09.162>.
- [14] REPETTE, W.L., MAILVAGANAM, N.P., “Calcium sulfoaluminate-based expansive admixtures – a review”, *American Concrete Institute*, v. 217, pp. 177–193, Jan. 2003.
- [15] LE SAOÛT, G., LOTHENBACH, B., HORI, A., *et al.*, “Hydration of Portland cement with additions of calcium sulfoaluminates”, *Cement and Concrete Research*, v. 43, pp. 81–94, Jan. 2013. doi: <http://dx.doi.org/10.1016/j.cemconres.2012.10.011>.
- [16] PILAR, R., FERRON, R.D., REPETTE, W.L., “Fresh properties of HPSCC containing SRA and expansive admixtures”, *Matéria*, v. 23, n. 3, e-12150, 2018. doi: <http://dx.doi.org/10.1590/s1517-707620180003.0484>.
- [17] PAN, Z., ZHU, Y., ZHANG, D., *et al.*, “Effect of expansive agents on the workability, crack resistance and durability of shrinkage-compensating concrete with low contents of fibers”, *Construction & Building Materials*, v. 259, pp. 119768, Oct. 2020. doi: <http://dx.doi.org/10.1016/j.conbuildmat.2020.119768>.
- [18] CHATTERJI, S., “Mechanism of expansion of concrete due to the presence of dead-burnt CaO and MgO”, *Cement and Concrete Research*, v. 25, n. 1, pp. 51–56, Jan. 1995. doi: [http://dx.doi.org/10.1016/0008-8846\(94\)00111-B](http://dx.doi.org/10.1016/0008-8846(94)00111-B).
- [19] RODRIGUES, P., “Aditivos expansores à base de óxido de cálcio supercalcificados”, *ANAPRE*, v. 10, n. 54, pp. 4, 2016.
- [20] NEVILLE, A.M., *Properties of concrete*, 4 ed., Essex, Longman Group Limited, 1995.
- [21] OLIVEIRA, M.J., RIBEIRO, A.B., BRANCO, F.G., “Combined effect of expansive and shrinkage reducing admixtures to control autogenous shrinkage in self-compacting concrete”, *Construction & Building Materials*, v. 52, pp. 267–275, Feb. 2014. doi: <http://dx.doi.org/10.1016/j.conbuildmat.2013.11.033>.
- [22] LI, J., ZHUANG, L., LIU, Z., *et al.*, “Evaluation of cracking in the shrinkage-compensating concrete with freeze–thaw resistance: from materials to structures”, *Materials and Structures*, v. 55, pp. 141, May. 2022. doi: <http://dx.doi.org/10.1617/s11527-022-01982-0>.
- [23] ZINGG, A., WINNEFELD, F., HOLZER, L., *et al.*, “Interaction of polycarboxylate-based superplasticizer and cements: influence of polymer structure and C<sub>3</sub>A content of cement”, In: *Proceedings of 12th International Congress on the Chemistry of Cement*, Montreal, 2007.
- [24] ZINGG, A., WINNEFELD, F., HOLZER, L., *et al.*, “Interaction of polycarboxylate-based superplasticizers with cements containing different C<sub>3</sub>A amounts”, *Cement and Concrete Composites*, v. 31, n. 3, pp. 153–162, Mar. 2009. doi: <http://dx.doi.org/10.1016/j.cemconcomp.2009.01.005>.

- [25] EVARISTO, W.F.O., ALMEIDA, V.L., CAPUZZO, V.M.S., “Influência do aditivo modificador de viscosidade nas propriedades do concreto autoadensável”, *Matéria*, v. 26, n. 3, e13050, 2021. doi: <http://dx.doi.org/10.1590/s1517-707620210003.13050>.
- [26] CHINAGLIA, D.L., GOZZI, G., ALFARO, R.A.M., *et al.*, “Espectroscopia de impedância no laboratório de ensino”, *Revista Brasileira de Ensino de Física*, v. 30, n. 4, pp. 4504, Dec. 2008. doi: <https://doi.org/10.1590/S1806-11172008000400013>
- [27] FAZZAN, J.V., SANCHES, A.O., AKASAKI, J.L., *et al.*, “Avaliação do caráter pozolânico da cinza do bagaço da cana-de-açúcar por meio de medidas de resistividade elétrica”, In: *Anais do 23º CBECiMAT – Congresso Brasileiro de Engenharia e Ciência dos Materiais*, v. 1, pp. 2955, Foz do Iguaçu, 2018.
- [28] RECH, G.L., PEROTTONI, C.A., “Python GUI for impedance spectroscopy analysis”, *Scientia cum Industria*, v. 6, n. 2, pp. 10–14, 2008. doi: <http://dx.doi.org/10.18226/23185279.v6iss2p10>
- [29] CABEZA, M., MERINO, P., MIRANDA, A., *et al.*, “Impedance spectroscopy study of hardened Portland cement paste”, *Cement and Concrete Research*, v. 32, n. 6, pp. 881–891, Jun. 2002. doi: [http://dx.doi.org/10.1016/S0008-8846\(02\)00720-2](http://dx.doi.org/10.1016/S0008-8846(02)00720-2).
- [30] DÍAZ, B., FREIRE, L., MERINO, P., *et al.*, “Impedance spectroscopy study of saturated mortar samples”, *Electrochimica Acta*, v. 53, n. 25, pp. 7549–7555, Oct. 2008. doi: <http://dx.doi.org/10.1016/j.electacta.2007.10.042>.
- [31] DEY, G., GANGULI, A., BHATTACHARJEE, B., *et al.*, “Electrical conductivity, dielectric permittivity, and degree of saturation of cement mortar at low radio frequencies”, *Journal of Testing and Evaluation*, v. 47, n. 4, pp. 2664–2880, Jul. 2018.
- [32] CARNOT, A., FRATEUR, I., ZANNA, S., *et al.*, “Corrosion mechanisms of steel concrete moulds in contact with a demoulding agent studied by EIS and XPS”, *Corrosion Science*, v. 45, n. 11, pp. 2513–2524, Nov. 2003. doi: [http://dx.doi.org/10.1016/S0010-938X\(03\)00076-3](http://dx.doi.org/10.1016/S0010-938X(03)00076-3).
- [33] GALLARDO, A.F.S., PROVIS, J.L.J., “Electrochemical cell design and impedance spectroscopy of cement hydration”, *Journal of Materials Science*, v. 56, n. 2, pp. 1203–1220, Jan. 2021. doi: <http://dx.doi.org/10.1007/s10853-020-05397-6>.
- [34] DONG, B., QIU, Q., XIANG, J., *et al.*, “Study on the carbonation behavior of cement mortar by electrochemical impedance spectroscopy”, *Materials*, v. 7, n. 1, pp. 218–231, Jan. 2014. doi: <http://dx.doi.org/10.3390/ma7010218>. PubMed PMID: 28788452.
- [35] AKHAVAN, A., RAJABIPOUR, F., “Evaluating ion diffusivity of cracked cement paste using electrical impedance spectroscopy”, *Materials and Structures*, v. 46, n. 5, pp. 697–708, Aug. 2013. doi: <http://dx.doi.org/10.1617/s11527-012-9927-x>.
- [36] HAMAMI, A.E.A., LOCHE, J.M., AÏT-MOKHTA, A., “Cement fraction effect on EIS response of chloride migration tests”, *Advances in Cement Research*, v. 23, n. 5, pp. 233–240, Oct. 2011. doi: <http://dx.doi.org/10.1680/adcr.2011.23.5.233>.
- [37] TAM, C.M., TAM, V.W.Y., NG, K.M., “Assessing drying shrinkage and water permeability of reactive powder concrete produced in Hong Kong”, *Construction & Building Materials*, v. 26, n. 1, pp. 79–89, Jan. 2012. doi: <http://dx.doi.org/10.1016/j.conbuildmat.2011.05.006>.
- [38] EID, J., TAIBI, S., FLEUREAU, J.M., *et al.*, “Drying, cracks and shrinkage evolution of a natural silt intended for a new earth building material. Impact of reinforcement”, *Construction & Building Materials*, v. 86, pp. 120–132, Jul. 2015. doi: <http://dx.doi.org/10.1016/j.conbuildmat.2015.03.115>.
- [39] ASSOCIAÇÃO BRASILEIRA DE NORMAS TÉCNICAS, *NBR NM 52 Agregado Miúdo – Determinação da Massa Específica e Massa Específica Aparente*, Rio de Janeiro, 2021.
- [40] ASSOCIAÇÃO BRASILEIRA DE NORMAS TÉCNICAS, *NBR NM 53 Agregado Graúdo – Determinação da Massa Específica e Absorção de Água*, Rio de Janeiro, 2021.
- [41] ASSOCIAÇÃO BRASILEIRA DE NORMAS TÉCNICAS, *NBR NM 248 Agregados – Determinação da Composição Granulométrica*, Rio de Janeiro, 2022.
- [42] CIMENTO ITAMBÉ, *Cimento certo*, <https://www.cimentoitambe.com.br/produtos/cp-v-ari/>, accessed in August 2020.
- [43] SOUZA, A.R., “*Retração em concreto autoadensável: contribuição de produtos mitigadores*”, Tese de M.Sc., Programa de Pós-graduação em Engenharia Civil, Universidade Tecnológica Federal do Paraná, Pato Branco, 2016.

- [44] ASSOCIAÇÃO BRASILEIRA DE NORMAS TÉCNICAS, *NBR 16889 Concreto – Determinação da Consistência pelo Abatimento do Tronco de Cone*, Rio de Janeiro, 2020.
- [45] ASSOCIAÇÃO BRASILEIRA DE NORMAS TÉCNICAS, *NBR 15823-2 Concreto Autoadensável Parte 2: Determinação do Espalhamento, do Tempo do Escoamento e do Índice de Estabilidade Visual – Método do Cone de Abrams*, Rio de Janeiro, 2017.
- [46] ASSOCIAÇÃO BRASILEIRA DE NORMAS TÉCNICAS, *NBR 15823-4 Concreto Autoadensável Parte 4: Determinação da Habilidade Passante – Método da Caixa L e da Caixa U*, Rio de Janeiro, 2017.
- [47] ASSOCIAÇÃO BRASILEIRA DE NORMAS TÉCNICAS, *NBR 16834 Concreto – Determinação da Variação Dimensional (Retração ou Expansão Linear)*, Rio de Janeiro, 2020.
- [48] ASSOCIAÇÃO BRASILEIRA DE NORMAS TÉCNICAS, *NBR 5738 Concreto – Procedimento para Moldagem e Cura de Corpos de Prova*, Rio de Janeiro, 2016.
- [49] ASSOCIAÇÃO BRASILEIRA DE NORMAS TÉCNICAS, *NBR 5739 Concreto – Ensaio de Compressão de Corpos de Prova Cilíndricos*, Rio de Janeiro, 2018.
- [50] AMERICAN SOCIETY FOR TESTING AND MATERIALS, *ASTM E1876 Standard Test Method for Dynamic Young's Modulus, Shear Modulus, and Poisson's Ratio by Impulse Excitation of Vibration*, West Conshohocken, 2021.
- [51] THINGIVERSE, *Impedance spectroscopy test apparatus*, <https://www.thingiverse.com/thing:4903062>, accessed in December, 2021.
- [52] CHRISTENSEN, B.J., COVERDALE, T., OLSON, R.A., *et al.*, “Impedance spectroscopy of hydrating cement-based materials: measurement, interpretation, and application”, *Journal of the American Ceramic Society*, v. 77, n. 11, pp. 2789–2804, Nov. 1994. doi: <http://dx.doi.org/10.1111/j.1151-2916.1994.tb04507.x>.
- [53] POPOVICS, S., “A model for the kinetics. of the hardening of Portland cement”, *Highway Research Record*, v. 192, pp. 14–35, 1967.
- [54] ASSOCIAÇÃO BRASILEIRA DE NORMAS TÉCNICAS, *NBR 15823-1 Concreto Autoadensável Parte 1: Classificação, Controle e Recebimento no Estado Fresco*, Rio de Janeiro, 2017.
- [55] PAN, Z., ZHU, Y., ZHANG, D., *et al.*, “Effect of expansive agents on the workability, crack resistance and durability of shrinkage-compensating concrete with low contents of fibers”, *Construction & Building Materials*, v. 259, pp. 119768, Oct. 2020. doi: <http://dx.doi.org/10.1016/j.conbuildmat.2020.119768>.
- [56] HAN, J., JIA, D., YAN, P., “Understanding the shrinkage compensating ability of type K expansive agent in concrete”, *Construction & Building Materials*, v. 116, pp. 36–44, Jul. 2016. doi: <http://dx.doi.org/10.1016/j.conbuildmat.2016.04.092>.
- [57] ZHAN, P.M., HE, Z.H., “Application of shrinkage reducing admixture in concrete: a review”, *Construction & Building Materials*, v. 201, pp. 676–690, Mar. 2019. doi: <http://dx.doi.org/10.1016/j.conbuildmat.2018.12.209>.
- [58] PILAR, R., SCHANKOSKI, R.A., FERRON, R.D., *et al.*, “Rheological behavior of low shrinkage very high strength self-compacting concrete”, *Construction & Building Materials*, v. 286, pp. 122838, Jun. 2021. doi: <http://dx.doi.org/10.1016/j.conbuildmat.2021.122838>.
- [59] POLAT, R., DEMIRBOGA, R., KHUSHEFATI, W.H., “Effects of nano and micro size of CaO and MgO, nano-clay and expanded perlite aggregate on the autogenous shrinkage of mortar”, *Construction & Building Materials*, v. 81, pp. 268–275, Apr. 2015. doi: <http://dx.doi.org/10.1016/j.conbuildmat.2015.02.032>.
- [60] COLLEPARDI, M., BORSOI, A., COLLEPARDI, S., *et al.*, “Effects of shrinkage reducing admixture in shrinkage compensating concrete under non-wet curing conditions”, *Cement and Concrete Composites*, v. 27, n. 6, pp. 704–708, Jul. 2005. doi: <http://dx.doi.org/10.1016/j.cemconcomp.2004.09.020>.
- [61] SEO, J.H., PARK, S.M., YANG, B.J., *et al.*, “Calcined oyster shell powder as an expansive additive in cement mortar”, *Materials*, v. 12, n. 8, pp. 1322, Apr. 2019. doi: <http://dx.doi.org/10.3390/ma12081322>. PubMed PMID: 31018545.
- [62] OLIVEIRA, M.J., RIBEIRO, A.B., BRANCO, F.G., “Strategies to mitigate shrinkage in an intermediate strength self-compacting concrete”, *Structural Concrete*, v. 22, n. S1, pp. E581–E595, Feb. 2021. doi: <http://dx.doi.org/10.1002/suco.201900456>.

- [63] TUTIKIAN, B.F., DAL MOLIN, D.C., *Concreto Autoadensável*, 2 ed., São Paulo, Pini, 2015.
- [64] KIOUMARSI, M., AZARHOMAYUN, F., HAJI, M., *et al.*, “Effect of shrinkage reducing admixture on drying shrinkage of concrete with different w/c ratios”, *Materials*, v. 13, n. 24, pp. 5721, Dec. 2020. doi: <http://dx.doi.org/10.3390/ma13245721>. PubMed PMID: 33333959.
- [65] SILVA, G.F., MARTINI, S., MORAES, J.C.B., *et al.*, “AC impedance spectroscopy (AC-IS) analysis to characterize the effect of nanomaterials in cement-based mortars”, *Construction & Building Materials*, v. 269, pp. 121260, Feb. 2021. doi: <http://dx.doi.org/10.1016/j.conbuildmat.2020.121260>.
- [66] OSF, *Influence of an over calcined calcium oxide-based shrinkage-compensating admixture on some properties of a self-compacting concrete*, <https://osf.io/3tynj/>, accessed in August, 2021.
- [67] STUTZMAN, P., “Scanning electron microscopy imaging of hydraulic cement microstructure”, *Cement and Concrete Composites*, v. 26, n. 8, pp. 957–966, Nov. 2004. doi: <http://dx.doi.org/10.1016/j.cemconcomp.2004.02.043>.